References

[1] L. Lauritson, G. J. Nelson, and F. W. Porto, "Data extraction and calibration of TIROS-N/NOAA Radiometers," NOAA Tech. Memo. NESS 107, p. 13.

[2] M. Wegener *et al.*, "Nontracking antenna systems for the acquisition of NOAA HRPT data," in *Proc. 3rd Nat. Space Symp.* (Canberra), pp. 238–240, 1987.

[3] "AVHRR phase demodulator, bit synchronizer, and frame synchronizer," Technical Description and Installation; Dept. Electrical Engineering, University of Dundee, Scotland, U.K.

Image Interpretation and Prediction in Microwave Diversity Imaging

HSUEH-JYH LI, NABIL H. FARHAT, AND YUHSYEN SHEN

Abstract—**The microwave image of a metallic object is interpreted from a new point of view, based on the understanding of the interconnection between the scattering mechanisms, the data acquisition system, and the image reconstruction algorithm. From this understanding we are able to interpret and predict microwave images reconstructed from data collected over specified and angular windows. The connection between a special scattering mechanism, edge diffraction, and its reconstructed image is established. The microwave image of an edge will be two bright points whose locations correspond to the end points of the edge if the normal aspect angle is not included in the angular windows; otherwise a line joining the two end points and representing the edge will appear in the image. Experimental images of a trihedral reflector reconstructed from data collected over different angular windows support this new approach to image interpretation and prediction.**

I. Introduction

Microwave diversity imaging is an imaging technique that exploits possible degrees of freedom, including spectral, angular, and polarization diversities [1]. In this imaging system, an object is seated on a rotating pedestal and is illuminated by a plane wave. For each aspect angle a set of pulses at different frequencies is transmitted and its echoes are received. The object is then rotated and the measurement is repeated to obtain the multiaspect stepped frequency response of the scattering object.

In the microwave regimes, the physical optics (PO) approximation is usually used to model the scattered field of a conducting object. It was shown that a three-dimensional (3-D) Fourier transform (FT) relationship exists between the shape of a perfectly conducting object and its backscattered far field under the PO approximation [2]. However, the PO approximation is inadequate for scattering problems of a complex shaped conducting object. At high-frequency edge diffractions, multiple reflections, creeping waves, and surface traveling waves are also important scattering mechanisms [3]. A field scattered from these scattering mechanisms cannot be treated by the PO approximation. Additionally, the spectral and angular windows for the data are usually restricted by practical constraints. Therefore, the microwave image of a metallic object might be different from its geometrical shape.

In this paper we will investigate microwave images of metallic objects employing microwave diversity imaging from a new point of view, based on the understanding of the interconnection between the object scattering mechanisms, the data acquisition system, and the image reconstruction algorithm utilized in image retrieval. The image reconstruction algorithm can be either the Fourier transform method or the back-projection method, and these two methods yield equivalent results [1], [4]. However, the back-projection method provides more physical insight into the image formation process [5]. Basically, the image is formed in three steps: 1) measure the scattered field over a specified spectral window and angular window; 2) obtain the range profile, which is the inverse FT of the range-corrected frequency response, at each aspect angle; and 3) back-project the range profile of each aspect angle onto an image plane to obtain the image. We will interpret and predict the microwave image based on the above three steps.

A different scattering mechanism might produce a different appearance in its microwave image. In this paper we will only deal with a special scattering mechanism—edge diffraction. For those objects consisting of conducting plates, edge diffractions are dominant contributors to the scattered field when the receiver is not in the specular direction of any one of the visible plates comprising the object. To a first order approximation the field scattered from the above type objects can be considered as a summation of the contributions from each "visible" plate, and the scattered field of a plate can be considered as a summation of the diffracted field from each "visible" edge. Therefore, diffraction from an edge is the basic building block for the scattering problem of those objects consisting of conducting plates.

In Section II the scattered field from an edge with finite length will be reviewed, the physical properties of its range profile will be explained, and the image formation for an edge with finite length will be discussed. A trihedral reflector is an object consisting of conducting plates. Experimental images of a trihedral reflector reconstructed from data collected over different angular windows will be demonstrated and interpreted in Section III.

II. Scattered Field, Range Profile, and Image Formation of a Finite Edge

Consider a conducting plate placed on a rotating pedestal as illustrated in Fig. 1. Points P_1 and P_2 are two vertices of the plate and the line P_1P_2 forms an edge of the plate. In the laboratory coordinate system, define the z-axis in the direction of the rotational axis, and the x-axis in the direction of the line of sight. At the starting angle the polar coordinates of the end points P_1 and P_2 are (r_1, θ_1, ϕ_1) and (r_2, θ_2, ϕ_2), respectively. As the plate is rotated with an angle ϕ the coordinates of P_1 and P_2 become $(r_1, \theta_1, \phi_1 + \phi)$ and $(r_2, \theta_2, \phi_2 + \phi)$, respectively. The differential ranges of these two end points at rotation angle ϕ are then $r_1 \sin\theta_1 \cos(\phi_1 + \phi)$ and $r_2 \sin\theta_2 \cos(\phi_2 + \phi)$, respectively. It is noted that the dependence of the differential ranges of the end points on the rotation angle is sinusoidal.

Next we define an edge-fixed coordinate for the plate. Let the z'-axis be in the direction of the edge P_1P_2, and the x'-axis be normal to the edge and lying on the plate surface. The corresponding inclination angle of the transmitter/receiver to the edge-fixed coordinate system is $\theta'(\phi = 0°)$. As the plate is rotated through an angle ϕ, the corresponding inclination angle for the edge-fixed coordinate system becomes $\theta'(\phi)$. It is noted that θ' is not only a function of ϕ but also a function of the orientation of the plate and the edge.

The diffracted field of a wedge with finite length for arbitrary incident and diffracted angles has been treated [6], where the con-

Manuscript received January 11, 1988; revised July 29, 1988. This work was supported by grants from the Army Research Office, the Scientific Research of Air, RCA, and GE Corporation.

H.-J. Li is with the Department of Electrical Engineering, National Taiwan University, Taipei, Taiwan, Republic of China.

N. H. Farhat is with The Moore School of Electrical Engineering, University of Pennsylvania, Philadelphia, PA 19104.

Y. Shen is with the Jet Propulsion Laboratory, California Institute of Technology, Pasadena, CA 91109.

IEEE Log Number 8823954.

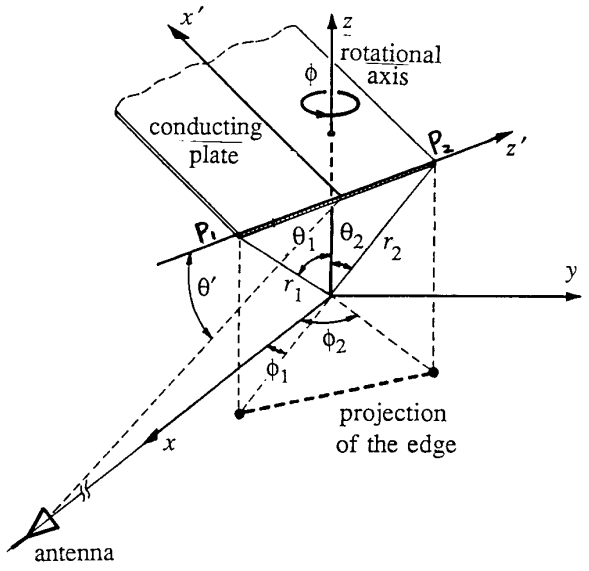

Fig. 1. Geometry and coordinates of an edge in the laboratory coordinate system and edge-fixed coordinate system.

cept of equivalent electrical current and equivalent magnetic current has been applied. Denote the equivalent electric current and equivalent magnetic current on the edge as $I(z')$ and $M(z')$. The expressions of I and M for the backscattering case can be found in [6]. They are functions of the inclination angle and the azimuth angle, and are inversely proportional to the wavenumber k.

The backscattered field of an edge with finite length L expressed in the edge-fixed coordinate system can be written by [6]

$$E_{\theta'} = \frac{j\omega\mu_0}{4\pi}\frac{e^{-jkr}}{r}\sin\theta' I(0) L \frac{\sin(kL\cos\theta')}{kL\cos\theta'} \quad (1)$$

$$E_{\phi'} = \frac{j\omega\mu_0}{4\pi}\frac{e^{-jkr}}{r}\eta\sin\theta' M(0) L \frac{\sin(kL\cos\theta')}{kL\cos\theta'} \quad (2)$$

where $I(0)$ and $M(0)$ are the equivalent electric current and equivalent magnetic current at $z' = 0$, and η is the characteristic impedance of the free space.

At a specific aspect the range profile is obtained by FT the range-corrected frequency response. After range correction (i.e., the first two terms on the right of (1) and (2) being removed), the range-corrected field can be further simplified to

$$E'_{\theta'} = \sin\theta' I(0) L \frac{e^{jkL\cos\theta'} - e^{-jkL\cos\theta'}}{2jkL\cos\theta'} \quad (3)$$

$$E'_{\phi'} = \eta\sin\theta' M(0) L \frac{e^{jkL\cos\theta'} - e^{-jkL\cos\theta'}}{2jkL\cos\theta'}. \quad (4)$$

The FT of (3) and (4) with respect to $2k$ over a finite bandwidth will give two peaks, located at range about $\pm(L/2)\cos\theta'$, which are at the differential ranges of the end points of the edge, with amplitude proportional to $I(0)$ or $M(0)$, and $1/(L\cos\theta')$ if $\theta' \neq 90°$. At the rotation angle ϕ such that $\theta'(\phi) = 90°$, the range profile gives a single peak with strong magnitude because the two end points of the edge have the same differential ranges and all the points on the edges are in equidistance to the observation point.

After realizing the aspect dependence of the range profile of the edge, we can then form and predict the image of an edge by the technique of back-projection [4], [5], [7]. After back-projection, the contributions of a specific range profile to the reconstructed image will be two parallel lines oriented in the direction of $\hat{\phi}$. Because the trace of each end point versus the rotation angle is sinusoidal, all back-projection lines for various rotation angles ϕ will pass through the corresponding end point as in the case of computer-aided tomography (CAT), intensifying the brightness of the end points. However, when the aspect such that $\theta'(\phi) = 90°$ is within the angular window (i.e., the aspect at which the incident wave is normal to the edge is contained within the angular window), the back-projection due to this range profile will be a single bright line.

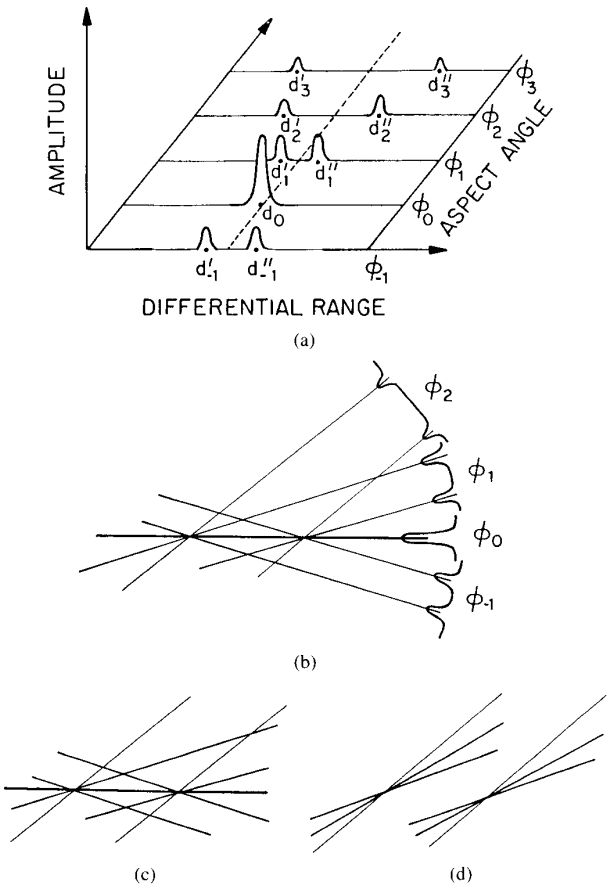

Fig. 2. Image formation of an edge. (a) Sketch of the range profiles of an edge at various aspect angles. (b) Implementation of the back-projection. Sketches of the images after back-projection (c) including and (d) without the aspect angle such that the edge is normal to the line of sight.

The above explanation is illustrated in Fig. 2. At rotation angle ϕ_0 the edge is normal to the line of sight (i.e., $\theta'(\phi_0) = 90°$), and the range profile for that aspect has a single peak with large amplitude. When the plate is rotated to another angle ϕ_i, the range profile has two peaks located at d_i' and d_i'' with smaller amplitudes (see Fig. 2(a)). The implementation of back-projection is illustrated in Fig. 2(b). The sketches of the image after back-projection including and excluding the specular aspect are shown in Fig. 2(c) and (d), respectively. The above discussions and illustrations indicate that the microwave image of an edge will be two bright points whose locations correspond to the end points of the edge if the normal aspect angle is not included in the angular window; otherwise a line joining the two points and representing the edge will appear in the image.

III. Microwave Images of a Trihedral Reflector

To verify the new interpretation approach, the microwave images of a trihedral reflector reconstructed from data collected over various angular windows are demonstrated below.

The geometry of a trihedral reflector and the imaging arrange-

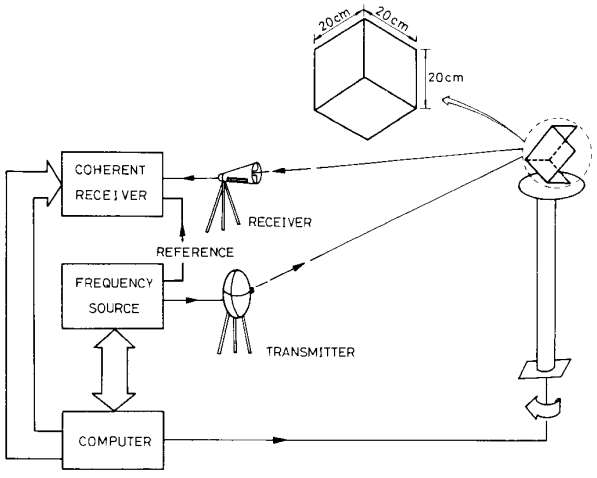

(a)

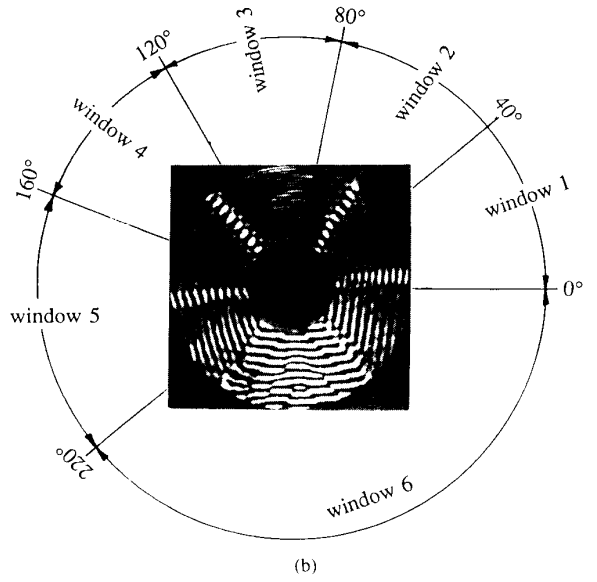

(b)

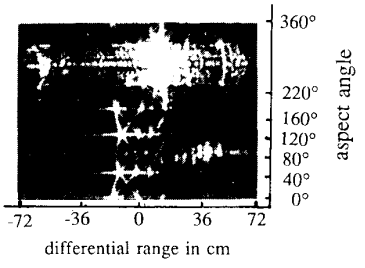

(c)

Fig. 3. Geometry, imaging arrangement, fringe pattern, and sinogram of a trihedral reflector. (a) Geometry and imaging arrangement of a trihedral reflector. (b) Real part of the range-corrected frequency response of the trihedral. (c) Sinogram of the trihedral reflector.

ment are shown in Fig. 3(a). The transmitting and receiving antennas have opposite senses of circular polarization. 101 equal frequency steps covering the 6–16.5 GHz range were used to obtain the frequency response of the trihedral reflector. The object is rotated clockwise 360°. The real part of the range-corrected complex

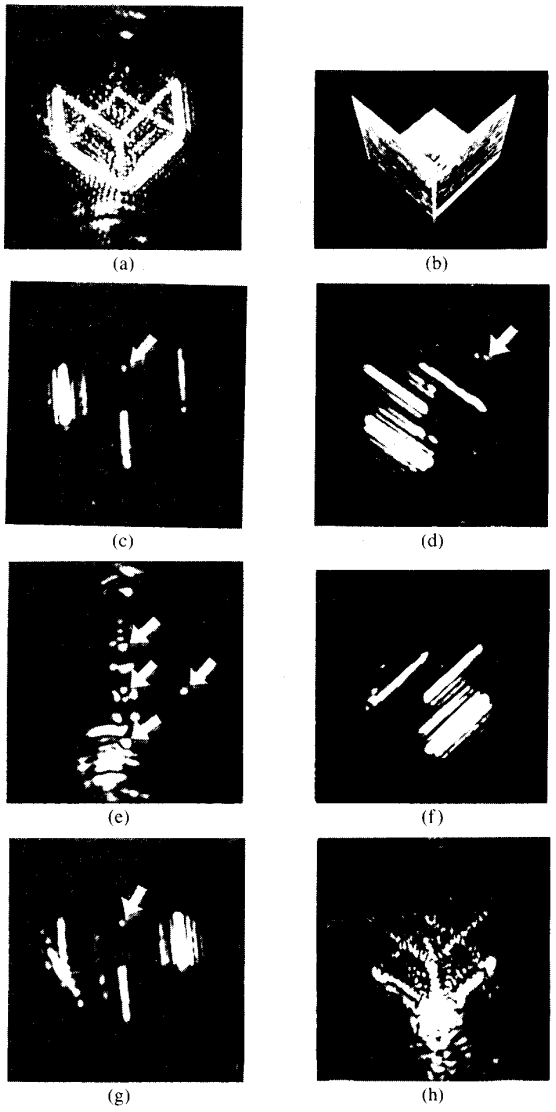

(a) (b) (c) (d) (e) (f) (g) (h)

Fig. 4. Photo image and microwave images of a trihedral reflector. (a) Microwave projective image reconstructed from data collected over angular window from $\phi = 0°$ to 220°. (b) Projective photo image. Microwave projective images reconstructed from data collected over (c) angular window 1 ($\phi = 0°$ to 40°); (d) angular window 2 ($\phi = 40°$ to 80°); (e) angular window 3 ($\phi = 80°$ to 120°); (f) angular window 4 ($\phi = 120°$ to 160°); (g) angular window 5 ($\phi = 160°$ to 220°); and (h) angular window 6 ($\phi = 220°$ to 360°).

frequency response of the trihedral reflector is shown as a central slice of Fourier data in Fig. 3(b). The radial distance of a given sample in this plot represents the frequency while the polar angle represents the rotation angle ϕ. The brightness of each point is proportional to the amplitude of the frequency response. The range profiles for all aspect angles are represented as a sinogram. The sinogram representation has been used in CAT [7] and is applied here to represent the range profiles of various aspect angles. It is a 2-D intensity varied display with the abscissa of the differential range, the ordinate of the aspect angle, and the intensity or brightness proportional to the amplitude of the range profile. The sinogram of the trihedral reflector is shown in Fig. 3(c). The bottom line represents the range profile of the first aspect ($\phi = 0°$) while the top line represents the range profile of the last aspect angle.

The magnitude of the range profile is proportional to the brightness of the display and the sinogram is displayed in linear scale. The dynamic display range has been suitably chosen so that weak signals will not be overridden. Examining the sinogram one can find that bright points are present in certain aspect angles. Locations of these bright points correspond to the differential ranges of the "visible" edges that are normal to the line of sight.

The image reconstructed through an angular window covering from $\phi = 0°$ to 220° is shown in Fig. 4(a). It is seen that the image is a projective image projected onto the plane normal to the rotational axis. The optical projective image is also shown in Fig. 4(b) for comparison. To verify our new image interpretation approach stated in the previous section, we divide the whole angular window into six subwindows and reconstruct the image from each subwindow. The resultant images are shown in Fig. 4(c)–(h). Examining the resultant images, one can find that only those edges that are normal to the line of sight within the specified angular window appear in the image. The brightness of the end points of the edges has been intensified. It is noted that no edges are normal to the line of sight in angular window 3. Accordingly, no edges are present in the image while the brightness of the vertices are intensified. Furthermore, the effect of multiple reflections is pronounced for some aspects in this window as can be seen from the fringe pattern (Fig. 3(b)) and the sinogram (Fig. 3(c)). Multiple reflection usually distorts the image because the range profile does not reflect the range information of the object shape [5], [8]. In angular window 6 strong multiple reflections are dominant contributors to the scattered field for most aspects. Although the edges can still be seen in the image, artifacts due to multiple reflections distort the image.

IV. Discussion and Conclusion

In this paper we interpret the microwave image of a metallic object from a new approach, based on the understanding of the interconnection between the scattering mechanisms, the data acquisition system, and the image reconstruction algorithm. From this understanding we can interpret and predict the microwave image reconstructed from data collected over specified spectral and angular windows. Experimental results support this new approach to image interpretation. Although the scattering mechanism treated in this paper is confined to the edge diffraction, the same approach can also be applied to establish the connection between the other scattering mechanisms and their reconstructed images [5]. Successful interpretation and prediction of the microwave image are fundamental to research in several areas, including target identification, classification, radar cross-section reduction, and image distortion [8].

References

[1] N. H. Farhat, C. L. Werner, and T. H. Chu, "Prospect for three-dimensional projective and tomographic imaging radar networks," *Radio Sci.*, vol. 19, no. 5, pp. 1347–1355, 1984.

[2] N. Bojarski, "Inverse scattering," Nav. Air Syst. Command, Warminister, PA, Final Rep. N000-19-73-C-0312F, Feb. 1974.

[3] G. T. Ruck, D. E. Barrick, W. D. Stuart, and C. K. Krichbaum, *Radar Cross Section Handbook*. New York: Plenum, 1970.

[4] N. H. Farhat and T. H. Chu, "Tomography and inverse scattering," *International Commission on Optics*, vol. ICO-13, pp. 62–63, 1984.

[5] H. J. Li, N. H. Farhat, Y. Shen, and C. L. Werner, "Image understanding and interpretation in microwave diversity imaging," *IEEE Trans. Antennas Propagat.*, to be published.

[6] A. Michaeli, "Equivalent edge currents for arbitrary aspects of observation," *IEEE Trans. Antennas Propagat.*, vol. AP-32, no. 3, pp. 252–258, 1984.

[7] G. T. Herman, Ed., *Image Reconstruction from Projections*. New York: Springer-Verlag, 1979.

[8] H. J. Li, N. H. Farhat, and Y. Shen, "Radar cross section reduction and image distortion employing microwave diversity imaging," submitted for publication.

Correction to "Effective Permittivity of Dielectric Mixtures"

ARI SIHVOLA AND JIN AU KONG

The following errors have been found in [1]:

Equation (11) should read

$$\epsilon_{\text{eff}}^{i} = \epsilon + \frac{f(\epsilon_s - \epsilon)\epsilon/[\epsilon + N_i(\epsilon_s - \epsilon)]}{1 - f(\epsilon_s - \epsilon)N_i/[\epsilon + N_i(\epsilon_s - \epsilon)]}$$

Equation (15) should read

$$\langle \bar{P} \rangle = \left(\bar{\bar{I}} - \frac{1}{\epsilon} \int_{4\pi} d\Omega n_0(\Omega) \bar{\bar{\alpha}} \cdot \bar{\bar{L}} \right)^{-1} \cdot \int_{4\pi} d\Omega n_0(\Omega) \bar{\bar{\alpha}} \cdot \bar{E}.$$

Manuscript received August 14, 1988.

A. Sihvola is with the Electromagnetics Laboratory, Helsinki University of Technology, Otakaari 5 A, SF-02150 Espoo, Finland.

J. A. Kong is with the Department of Electrical Engineering and Computer Science, Research Laboratory of Electronics, Massachusetts Institute of Technology, Cambridge, MA 02139.

IEEE Log Number 8824341.

Equation (21) should read

$$\epsilon_{\text{eff}} = \epsilon + \frac{\sum_{i=1}^{3} \frac{f\epsilon(\epsilon_s - \epsilon)}{3[\epsilon + N_i(\epsilon_s - \epsilon)]}}{1 - \sum_{i=1}^{3} \frac{fN_i(\epsilon_s - \epsilon)}{3[\epsilon + N_i(\epsilon_s - \epsilon)]}}.$$

Equation (23) should read

$$\bar{\bar{\alpha}} = v_0(\epsilon_s - \epsilon) \sum_{i=1}^{3} \frac{\epsilon_a}{\epsilon_a + N_i(\epsilon_s - \epsilon)} \hat{u}_i \hat{u}_i.$$

The last formula in the first column of page 423 should read plainly

$$\epsilon_{\text{eff}} = \epsilon + \frac{f}{3}(\epsilon_s - \epsilon) \sum_{i=1}^{3} \frac{\epsilon_{\text{eff}}}{\epsilon_{\text{eff}} + N_i(\epsilon_s - \epsilon_{\text{eff}})}.$$

Lines 19 and 20 on the second column on p. 423 should read "For aligned ellipsoids with $\epsilon_a = \epsilon_{\text{eff}}$, we find the coherent potential formula . . .".

Equation (31) should read

$$\epsilon_{\text{eff}} = \epsilon + \frac{\frac{1}{3}\sum_{j=1}^{n} f_j(\epsilon_j - \epsilon) \sum_{i=1}^{3} \frac{\epsilon}{\epsilon + N_{ji}(\epsilon_j - \epsilon)}}{1 - \frac{1}{3}\sum_{j=1}^{n} f_j(\epsilon_j - \epsilon) \sum_{i=1}^{3} \frac{N_{ji}}{\epsilon + N_{ji}(\epsilon_j - \epsilon)}}$$